Space-Filling Curve Radio Frequency Identification Tags

John A. McVay[1], Ahmad Hoorfar[2] and Nader Engheta[3]

[1]Eureka Aerospace
Pasadena, CA, 91067

[2]Department of Electrical and Computer Engineering
Villanova University, Villanova, PA 19085

[3]Department of Electrical and System Engineering,
University of Pennsylvania, Philadelphia, PA 19104

Abstract- Two different concepts for the use of resonant space-filling curves (SF-curves) elements as RFID tags are proposed. In the first concept the space-filling curve geometries such as Hilbert and Peano curves are studied with respect to the creation of an ultra-passive type of RFID in which an array of space-filling curve elements, scaled to resonate at different and particular frequencies, are used to provide a backscattered signal, in which information can be embedded. Using both numerical simulations and RCS measurement, it is shown that these electrically compact resonators could produce relatively large scattered fields over an inherently narrow frequency band at their corresponding fundamental resonant modes. The performances of these tags are also investigated when placed near a typical inventory objects, such as paper rolls. In the second concept, an SF-curve antenna is used above an SF-curve high impedance surface to develop an RFID tag that is well-suited for tagging of conducting objects.

Index Terms- RFID, passive tags, SF curves.

I. INTRODUCTION

In recent years, there has been considerable interest in the area of Radio Frequency Identification (RFID) and Radio Frequency Tagging (RFTAG). This emerging area of technology has a wide range of applications that include commercial inventory control in warehouses, supermarkets, hospitals as well as in military friend/foe identification to name but a few [1-2]. Most of these applications require low cost, thin-film printed antennas and sensors. The current technology can be broken down into two main groups, namely passive and active RFID tags. In general, both active and passive tags utilize integrated circuits, with active tags utilizing a source, such as a battery. In passive RFID tags, the electrical current induced in the antenna by the incoming radio frequency signal provides just enough power for the integrated circuit (IC) in the tag to power up and transmit its response. Most passive tags emit signal by backscattering the carrier signal from the reader. This means that the antenna has to be designed to collect its power from the incoming signal as well as transmit the response signal. The lack of an onboard power supply means that the device can be quite small. Passive tags have practical read distances ranging from about 2 mm up to a few meters depending on the radio frequency and antenna design, type and/or size. Passive RFID tags can be much smaller and cheaper to manufacture than their semi-passive, which uses a small battery, and active counterparts and can have an almost unlimited life span. Majority of RFID tags in existence are of the passive variety.

This work explores the potential for utilizing the electrically small, resonant characteristics of space-filling curves (SF-curves) [3] for RFID technologies. An interesting property of a space-filling curve, such as Peano and Hilbert curves, shown in Fig. 1, is that, as the higher iteration-orders, n, of this curve are considered, a long "line" can be compacted into a small "surface" area. In general, the expressions relating total lengths, S_H and S_P, of the Hilbert and Peano curves to their corresponding side dimension, L, are:

$$S_H = \left(\frac{2^{2n}-1}{2^n-1}\right)L \;\; ; \; S_P = \left(\frac{3^{2n}-1}{3^n-1}\right)L \, . \tag{1}$$

From an electromagnetic point of view, such a curve may provide a structure that, although small in its footprint, can be resonant at a wavelength much longer than its footprint. Such a "compact resonator" can be quite useful in various applications in radiation and scattering problems. For instance, this feature is of interest to antenna designers since it provides a planar resonant radiator that can have a very small footprint as one considers the higher orders in iterative filling of a 2-D region [4-8]. These curves have also been utilized as inclusions to form high impedance ground-planes (HIGP), also known as artificial magnetic conductors (AMC) [11, 12].

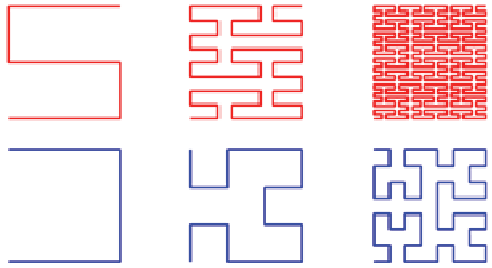

Fig. 1. First three orders of Peano (top) and Hilbert (bottom) space-filling curves.

In particular, we present two different concepts for the use of the SF-curves as RFID tags. In the first concept the space-filling curve geometries are studied with respect to the creation of an ultra-passive type of RFID in which an array of space-filling curve elements, scaled to resonate at different and particular frequencies, are used to provide a backscattered signal, in which information can be embedded. In the second concept, an SF-curve antenna [6, 8] is used above an SF-curve high impedance surface, or artificial magnetic conductor (AMC) [11, 12] to develop a tag that is well-suited for tagging of conducting objects, which, as it is well known, causes very poor performance when conventional RFID tags are used. Previous works [6, 8, 11, 12] have shown that for a given footprint the Peano of order 2 and the Hilbert of order 3, resonate approximately at the same fundamental resonant frequency with a similar relative bandwidth, which is why, in this work, these two orders are often compared side-by-side.

II. PRINTED PEANO AND HILBERT ARRAYS FOR RFID TAGS

The "compact resonator" behavior of the Peano and Hilbert curves may allow for relatively small resonant passive tags with comparably large scattering characteristics. The relatively narrow bandwidth inherent to these geometries may prove useful in allocating the narrow resonances as the "spectral ID". To investigate the scattering characteristics of these curves, a single element Peano curve of order 2 and single element Hilbert curve of order 3, both contained within a 30 mm x 30 mm footprint (linear side-dimensions), were studied in free-space under the influence of a normally-incident, uniform plane-wave excitation with varying frequency, utilizing a method of moments (MoM) code, NEC-4. The corresponding mono-static radar cross-section (RCS), as a function of frequency, and the scattering RCS patterns are shown in Figs. 2 and 3, for the Peano curve and the Hilbert curve element, respectively. Two different polarizations were studied corresponding to polarizations in the x and y-directions, Ex and Ey, respectively. As can be seen, both curves possess resonances dependent on the polarization of the excitation, and at the resonances, the scattering from the curves behave like resonant dipoles, and yet the 30 mm × 30 mm footprint which encloses these curves is electrically very small with respect to the resonant wavelengths. For the fundamental resonance corresponding to the y-polarized excitation, both the Peano and Hilbert curves have electrical footprints on the order of 0.07λ. Since the curves are smallest with respect to this first resonance, corresponding to the y-polarized electric field excitations, the primary focus of the work presented here will focus on this lowest resonance.

We now consider the space-filling curve geometries in creation of an ultra-passive type of RFID in which an array of space-filling curve elements, scaled to resonate at different and particular frequencies, are used to provide a backscattered signal, in which information can be embedded.

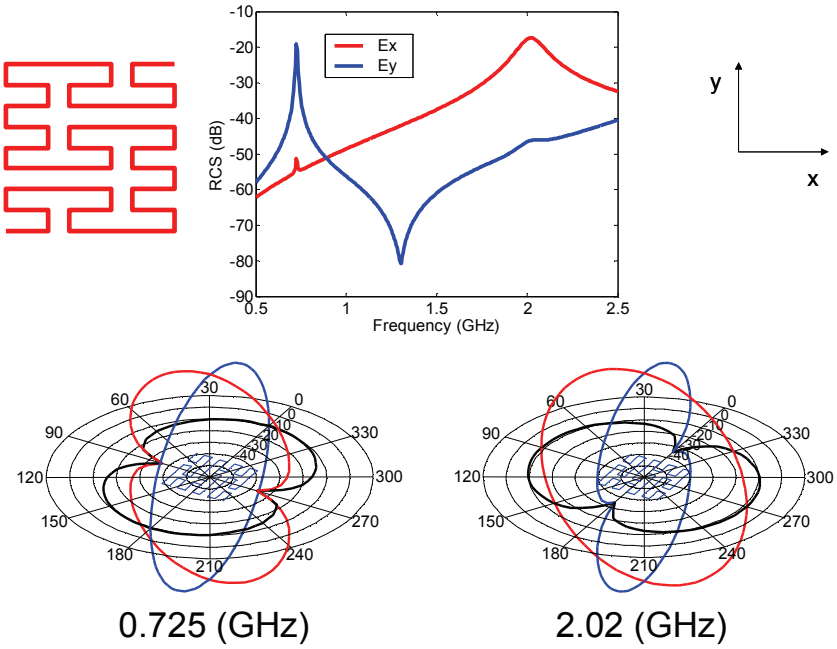

Fig. 2. Results of numerical simulations for scattering from a single Peano of order 2 element.

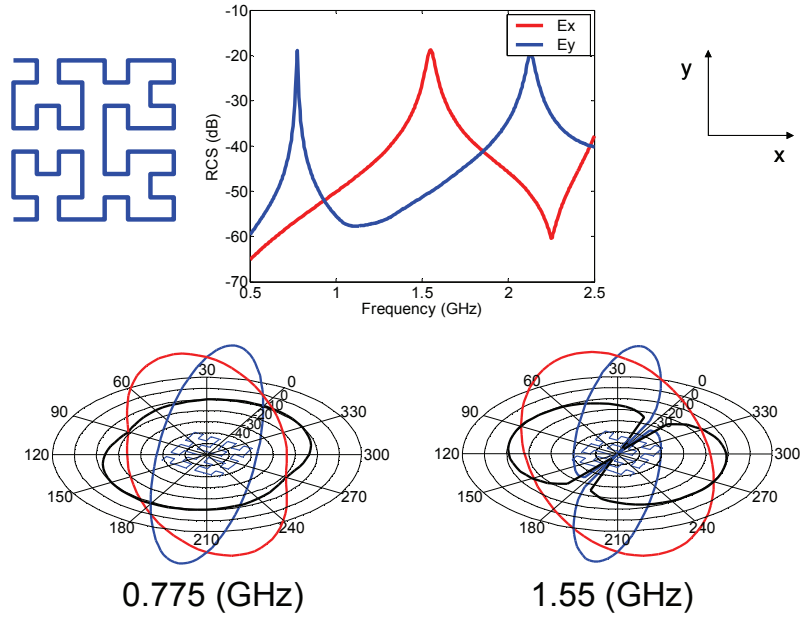

Fig. 3. Results of numerical simulations for scattering from a single Hilbert of order 3 element.

To illustrate a potential RFID tag application, a 5-element array of Peano and Hilbert curve scatterers, shown in the insets of Figs. 4-5 (Peano) and 6-7 (Hilbert), are examined, respectively. For the case of the Peano array, each element consists of a Peano curve of order 2 while in the cases of the Hilbert array, each element consists of a Hilbert curve of order 3. Each element within the array is scaled to 95% of the physical size (e.g. footprint) of the element to its left and by using this scaling factor, each element in the array is designed to resonate at a separate and particular frequency. When illuminated with a normally incident plane-wave excitation, polarized in the x

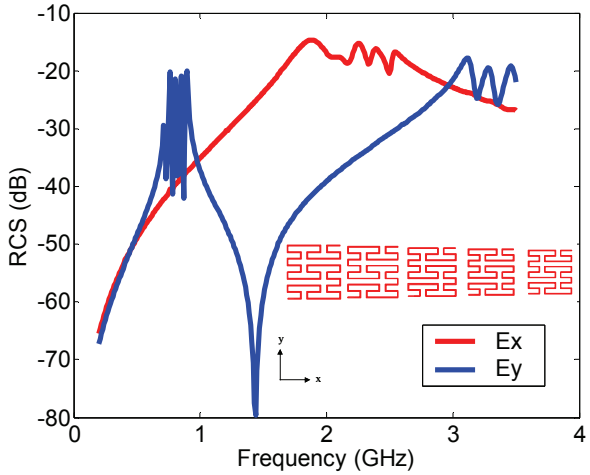

Fig. 4. Frequency signature for 5-element Peano RFID tag (inset) for both polarization excitations.

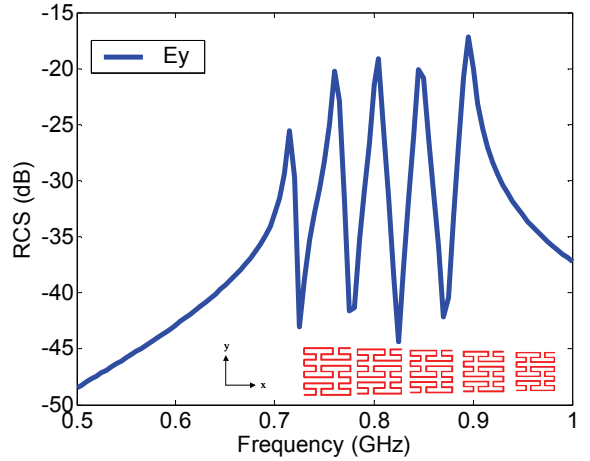

Fig. 5. Expanded (zoomed in) E_y frequency signature for 5-element Peano RFID tag, shown in inset.

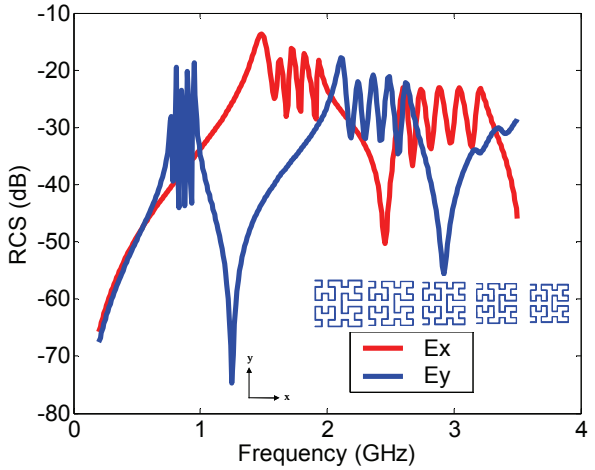

Fig. 6. Frequency signature for 5-element Hilbert RFID tag (inset) for both polarization excitations.

and y-directions separately (see Figs. 4 (Peano) and 6 (Hilbert)), these geometries give rise to the scattering shown in the respective figures. Multiple peaks in the Radar Cross Section (RCS) are evident and each peak corresponds to the resonance of a different element within the array. For this illustration, the arrays were designed to produce a mono-static RCS representative of the binary number 11111, where a peak in the RCS refers to a binary 1. It is in this manner that the Peano and Hilbert arrays are acting like a bar-code, as is used in the optical regime, but instead the information is contained within the frequency response of the tag.

From Figs. 4 and 6 it is noted that the frequency response is different for both of these arrays, for the x-polarized and y-polarized incident fields used to excite these structures. For the x-polarized case, the elements in the arrays achieve resonance at higher frequencies and thus the element sizes are larger with respect to the operational wavelength. Also, since the higher order resonances possess a larger relative bandwidth, the total frequency spectrum occupied by the RFID tag is greater (e.g. less compact).

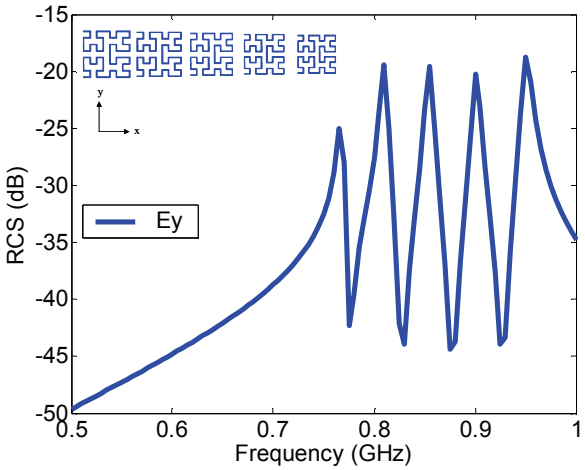

Fig. 7. Expanded (zoomed in) E_y frequency signature for 5-element Hilbert RFID tag, shown in inset.

III. POLARIZATION INDEPENDENT TAGS

To address the issue of the polarization dependence on such tags, the geometry shown in the inset of Fig. 8 is considered. In this geometry, consisting of Hilbert curves of order 3, each

element within the previous array is replaced with 4-elements, identical in size with the original, 2 of which are rotated by 90° with respect to the original element. This process is repeated for each element and again the 95% scaling factor is applied to each super-element. In the case shown in Fig. 8, again a 5-element array was assumed and then the second and forth elements were removed to produce a signature of 10101. This frequency signature is now obtained regardless of the polarization of the incoming excitation albeit at the expense of tag elements which are larger in size. Due to coupling among the elements, the frequency response is not completely independent on polarization, but the dependence on polarization has been significantly reduced.

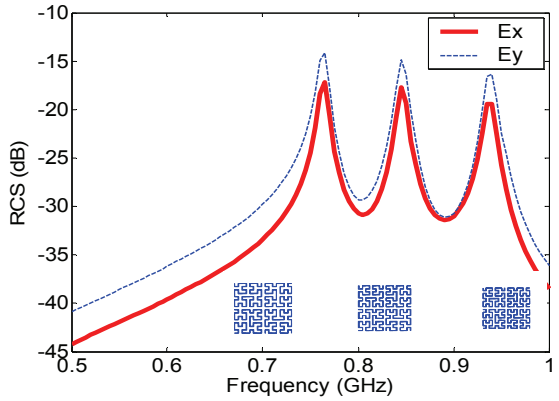

Fig. 8. Frequency signature for a Hilbert RFID tag with reduced polarization sensitivity.

IV. PEANO RFID TAG ON A DIELECTRIC AND METALLIC CYLINDER

To investigate the performance of the proposed space-filling RFID tags when placed near a typical inventory object, Finite Element Method (FEM) based HFSS software was used to numerically model the radar cross-section (RCS) of the 5-element array of Peano-curve elements of 2nd order on a paper roll (see Fig. 9). The paper roll was assumed to have $\varepsilon_r = 2.6$, $\tan\delta = 0.08$ as given as appropriate values in [9]. The 5-element Peano array is identical to the previously studied case (see Figs. 4 and 5) however now the array is considered as printed on a Duroid substrate with a thickness of 1.575 mm which accounts for a slight shift in frequency as compared to the free-space case considered previously in Fig. 5. Various radii of the paper roll were considered to investigate the performance of the RFID tag in the presence of both large and small inventory objects. The height of the paper roll was fixed at 210 mm for all cases and the electric field of the incident plane-wave was polarized in the direction of the cylinder axis.

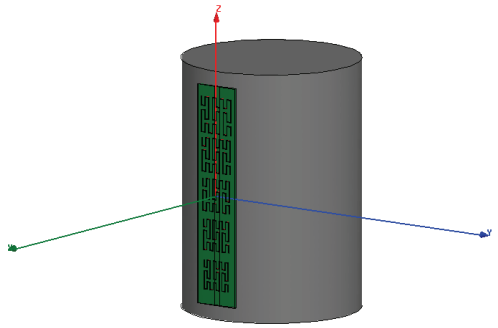

Fig. 9. The Peano-curve array placed on a paper roll of height 21 cm and radius r.

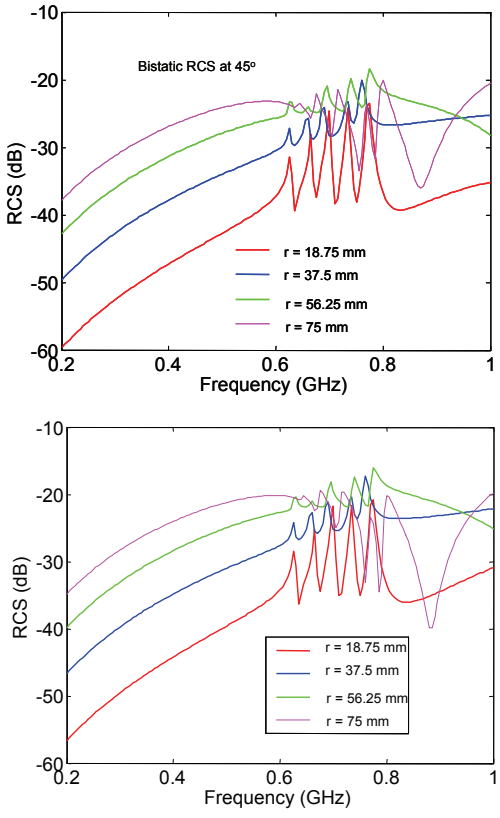

Fig. 10. Results of numerical simulation for the RCS of the Peano-curve RF tag near a paper roll for different radius values.

The monostatic and bistatic RCS results for the paper rolls of various radii are plotted in Fig.

10. The backscattered and the bistatic results at 45 degrees are very similar, due to the dipolar scattering pattern associated with these elements, as shown in Fig. 11 for the resonance at 0.76GHz.. For the cases of r = 18.75 mm and r = 37.5 mm, one can clearly see the peaks corresponding to the resonant frequencies of the Peano curve elements, and hence the RFID tag frequency signature. As the radius of the paper roll increases, however, the resonant peaks become less pronounced due to the increased contribution of the paper roll to the overall RCS of the combined geometry.

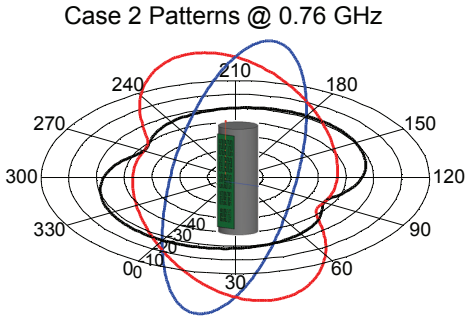

Fig. 11. Scattering Patterns of the Peano-curve RF tag on a paper roll of 37.5mm radius at 0.76GHz.

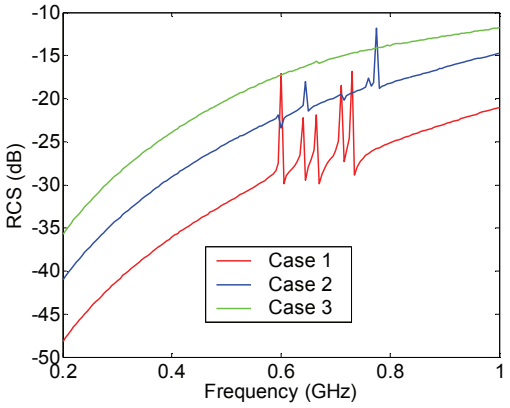

Fig. 12. Monostatic frequency signatures for cases shown in Fig. 8.6 but when the cylinder is considered as metallic (radii = 18.75 mm (case 1), 37.5 mm (case 2) and 56.25 mm (case 3).

This effect was also found, and even more pronounced when a metallic cylinder made of aluminum was considered in place of the paper roll cylinder. The scattering for the case when the cylinder is metallic is shown in Fig. 12. For this case, it can be seen that the scattering from the tagged object, namely the metallic cylinder, completely dominates the return by the third case studied. To this end, the possibilities into the use of space-filling curve RFID tags for tagging large metallic objects are investigated in a later section. Background subtraction or other appropriate signal processing algorithms may also potentially be used to enhance the peaks in the received RCS spectrum.

IV. EXPERIMENTAL RESULTS

In order to experimentally confirm the overall space-filling curve RFID tag concept, a set of 3-element arrays, corresponding to the Peano order 2 and Hilbert order 3 geometries, and a 5 element array of 3rd order Hilbert curve elements were fabricated (see Fig. 13 insets). In both the Peano and Hilbert RFID tag cases the largest tag element was scaled such that the lowest resonant frequency was within the frequency range of the available horn antennas (1-12.4 GHz) utilized for the measurement and as such, the dielectric substrate effects were also taken into account in the design. The largest element size for both the Peano and Hilbert tag arrays is about 7 mm. The subsequent elements were then scaled using a 95% scaling factor as was previously discussed. The arrays were fabricated on DUROID 5870 (ε_r=2.33) and measured. The measurement setup consisted of two H-1479 horns, one for transmit and one for receive, with a 267 mm separation distance between them. The RFID tags were placed, separately, 122 cm downrange. The RCS was collected utilizing an Agilent E-5071B vector network analyzer and some absorbing material was utilized to reduce noise and reflections within the room. Measurements were taken both in the absence of and in the presence of the RFID tags in order to perform background subtraction. The RCS results are plotted in Fig. 13, for both tags utilized. The peaks corresponding to the resonant frequencies, f_1, f_2 and f_3, of the space-filling curve elements can be seen. A similar 5-element Hilbert array was also fabricated and its measured RCS is shown in Fig. 14.

V. LOCATING MULTIPLE NEARBY TAGS

One potential pitfall for this type of ultra-passive tag would be the ability to identify

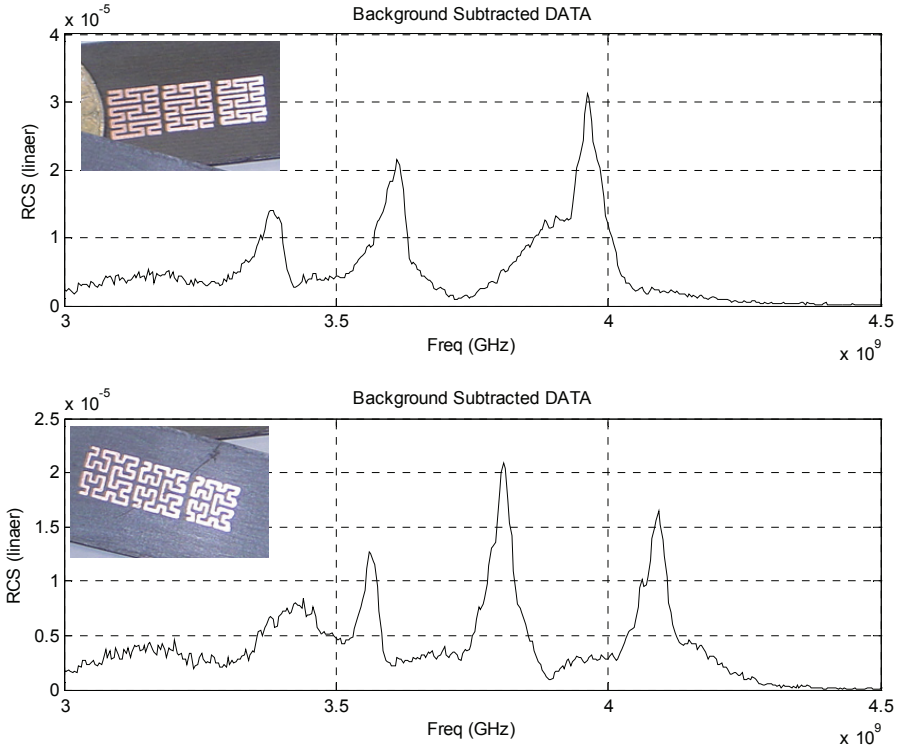

Fig. 13. Measured frequency signature for 3-element Peano and Hilbert RFID tags.

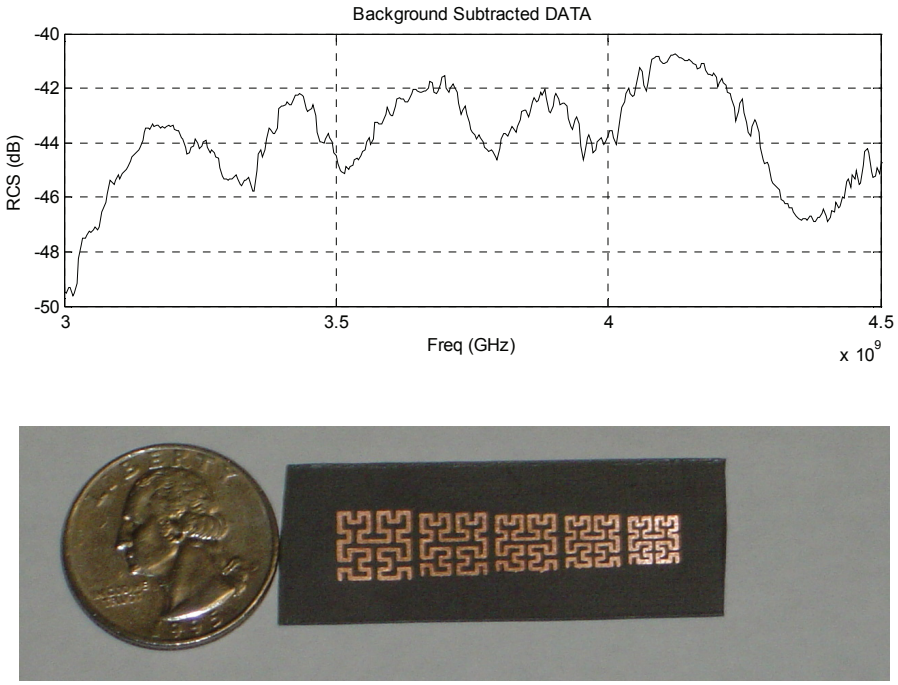

Fig. 14. Measured frequency signature for 5-element Hilbert RFID tag.

multiple tags located within close proximity to one another. Passive and active tags offer the advantage that a given tag can be "silenced" while another tag is "interrogated". However, in this section delay and sum beamforming is explored as an approach that may allow for the frequency

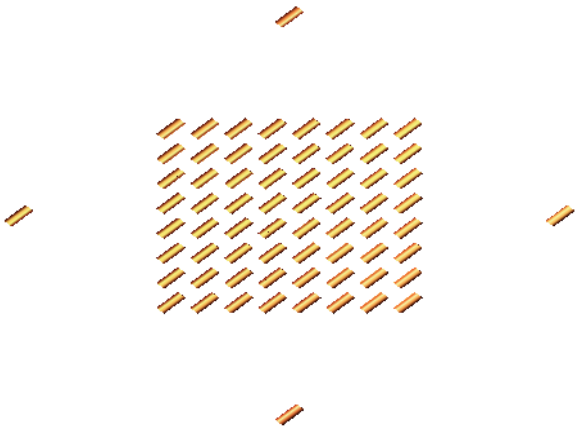

Fig. 15. Rectangular array of dipole elements; 64 receive elements and 4 transmit elements.

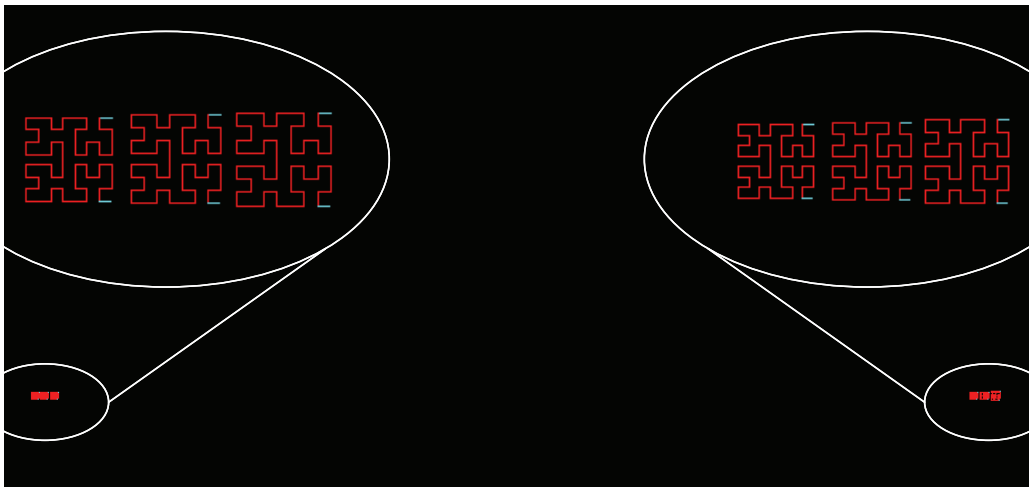

Fig. 16. Two separate Hilbert curve RFID tags.

signature of multiple tags within close proximity to be extracted.

Using Method of Moment based NEC-4, a receive array consisting of a rectangular array of 64 dipole elements is numerically modeled. Fourtransmit dipole elements are placed near the receive array. The geometry of the array is shown in Fig. 15. The elements in the receive array are spaced ½ λ apart (at 2.5 GHz) and are λ/2 dipoles. The 45 degree rotation of the elements is to avoid contact between the elements. The transmit elements are placed 4.5 times the separation distance of the receive elements, away from the rectangular array sides. This particular set-up was chosen to correspond to a particular array, in use for another unrelated radar project that has been proven effective in imaging of nearby objects in a cluttered environment [10].

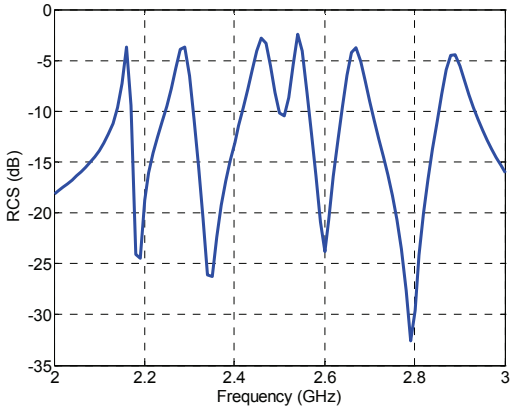

Fig. 17. Numerically calculated received signal without delay and sum beamforming.

Two separate 3-element space-filling curve tags were then modeled and placed 3.2 meters

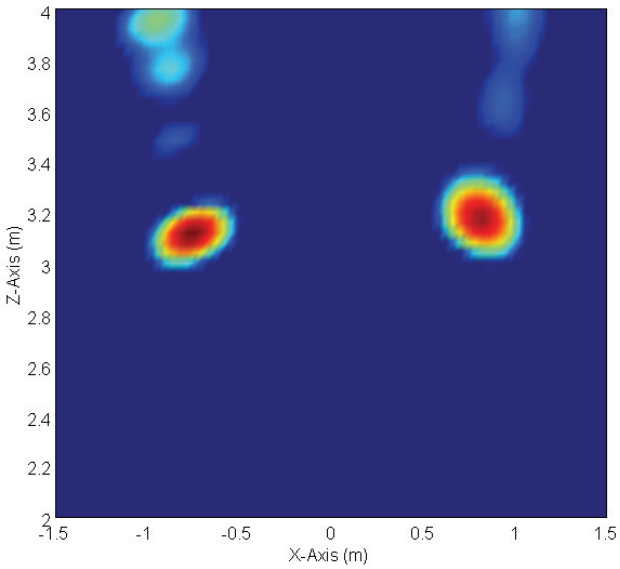

Fig. 18. Results of numerical simulations for the output of the beamformer in the area of interest. The "hot spots" correspond to the returns from the space-filling curve RFID tags.

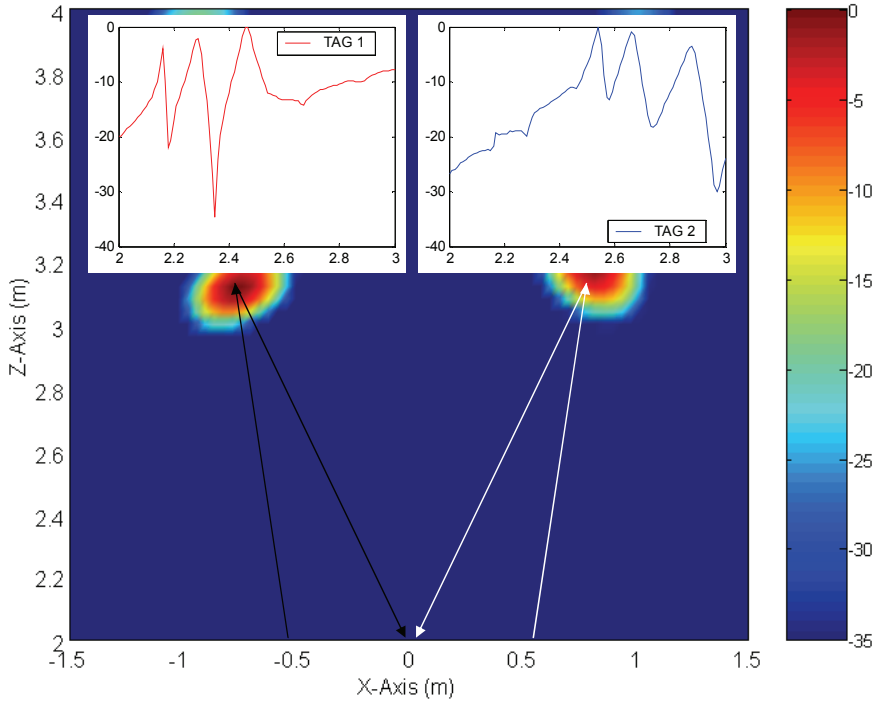

Fig. 19. Simulation results: Application of the proper phase delays in the directions of the targets to obtain the frequency content at the desired locations. Insets show the frequency content of the individual tags, separated by the process described in the text.

downrange of the array. The model for the tags is shown in Fig. 16.

The numerically calculated received signal without any processing is shown in Fig. 17. As can be seen, 6 peaks are present, however it is not evident which peak corresponds to which tag. Beamforming is then implemented over the frequency range from 1 to 3 GHz. To implement the beamformer, the delay path for a single transmit/receive path was calculated and applied

for each transmit/receive pair, for all the pixels within the space being imaged. The space imaged was 3 meters by 3 meters with a separation of 0.04 m between the individual (pixel) locations being imaged in both x and y directions. The standard beamforming equation is given by:

$$I(l,m,n) = \sum_{p=1}^{P} \sum_{q=1}^{Q} \sum_{k=1}^{K} R_{pq}(\omega_k) e^{j\omega_k \tau_{pq}(l,m,n)} \quad (2)$$

where $I(l,m,n)$ is the total power received at the pixel location (l,m,n), k corresponds to the sum across the frequency range, p and q correspond to the transmit receive pair, respectively and the exponential term $e^{j\omega_k \tau_{pq}(l,m,n)}$ gives the focusing delay for the location (l,m,n) at the k^{th} frequency for the pq receive pair, where $\tau_{pk}(l,m,n)$ is the phase delay between the pq receive pair to the location (l,m,n). Rpq is the received signal from the pth transmitter to the qth receiver.

The resulting output of the beamformer is shown in Fig. 18. The "hot spots" shown correspond to the locations of the two separate tags.

In order to obtain the separate frequency responses, the S-parameter data collected in the above procedure can then be focused in the direction of one particular tag and the sum over the frequency range in (2) can be omitted in order to obtain frequency information content from that particular location, while simultaneously spatially filtering out signals arriving from other locations. Applying this procedure for each of the "hot spots" in Fig. 18, the frequency content is extracted and shown in Fig. 19.

VI. HILBERT-CURVE RFID ANTENNA ABOVE HILBERT-CURVE HIGH-IMPEDANCE GROUND-PLANE

It is well known that a horizontally polarized radiating element will not radiate efficiently when placed horizontally above and within close proximity to a good conductor. If however an artificial magnetic conductor could be realized, it could be used to enhance the radiation characteristics of the radiating element. In this section we study the potential of utilizing the electrically small SF-curve radiating elements, above the high impedance ground-planes (HIGP), also known as artificial magnetic conductors (AMC) made of space-filling curve inclusions [11, 12]. In such a process, it may be possible to have an electrically small yet resonant, horizontal, dipole-like element within close proximity to a conductive ground-plane, while maintaining a matched system with gain values greater then that of the free-space counterparts. Such a scheme may particularly be useful when these antennas are used in RFID tagging of conducting objects in either passive or an active RFID application.

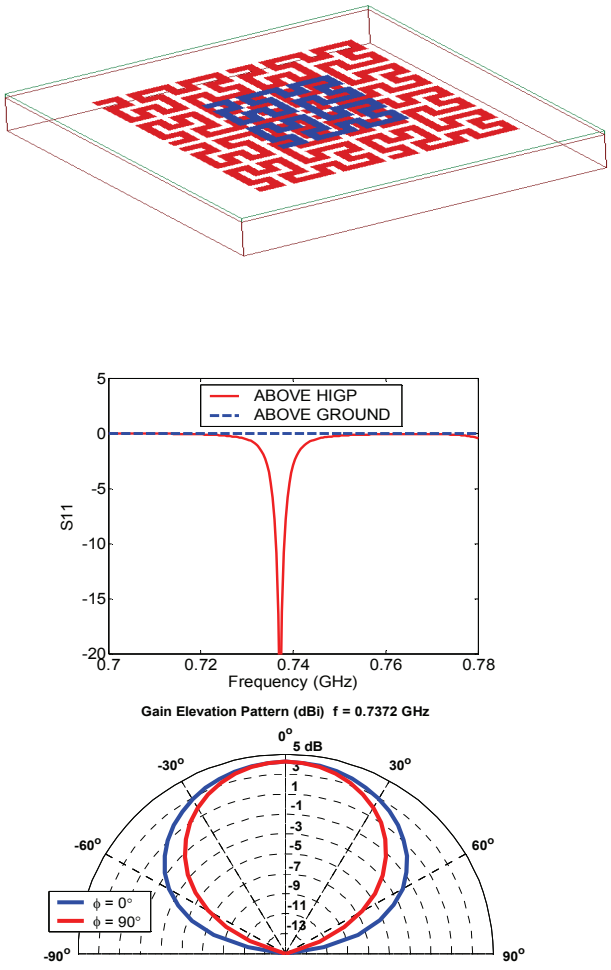

Fig. 20. Hilbert RFID tag utilizing a Hilbert HIGP (AMC) for enhanced radiation performance.

As an example we consider the case shown in Fig. 20. It consists of a Hilbert curve of order 3 antenna, matched in free-space to a 50 Ω source by judiciously choosing its feed location [6]. When placed at a height of 15 mm above a conductive ground, of infinite extent, it gives rise

to the return loss (S11) shown in Fig. 20 (blue, dashed line). As can be seen, in the presence of the metallic ground, the match to the 50 Ω source is lost, due to the small value of radiation resistance when in close proximity to the conductive backing. When a 2 by 2 array, also consisting of Hilbert curves of order 2, acting as a high-impedance ground-plane is inserted between the antenna and the ground plane, at a height of 13.425 mm, the radiation resistance is restored as is the 50 Ω source match as is evident in the return-loss values plotted in Fig. 20, as a function of frequency, for the antenna above the high-impedance ground plane. The gain elevation pattern, corresponding to the resonance is also shown in Fig. 20 and it is noted that the pattern is similar to a dipole pattern, in the presence of a conductive ground of infinite extent and that the gain of the antenna, in the presence of the AMC is on the order of 4.26 dBi.

In order to provide an experimental verification of the proposed space-filling curve dipole antenna above the corresponding high-impedance ground-plane, a realistic feed system must first be considered. In the numerical modeling, one can simply assume a 50Ω gap-source, while in practice; this requires a bit more thought. Since this system has a ground-plane, a coaxial-probe fed system is considered, as is utilized in many patch antenna designs. Since this design consists of 3 layers, a ground-plane, a high-impedance surface and a dipole layer, it will be necessary to feed a probe up from the ground-plane to the antenna layer. A commonly used SMA probe diameter is 1.27 mm. In order to feed the probe through the surface without making an electrical connection, the inclusions on the high-impedance surface must be scaled such that a 1.27 mm probe can fit in between the distances between the inclusions' microstrip lines.

An SMA coaxial probe is grounded to the ground-plane while the probe center comes up through the high-impedance surface and connects to the antennas' 50Ω free-space feed location. The numerical model of the coaxial-fed antenna is shown in Fig. 21. The shaded areas correspond to the 1.575 mm thick Duroid (ε_r=2.2) substrates which were also considered in the modeling process. We note that for a passive tag when an IC chip is connected in place of the probe, the antenna should be matched to the input-impedance of the chip by choosing an appropriate feed-point location on its trace.

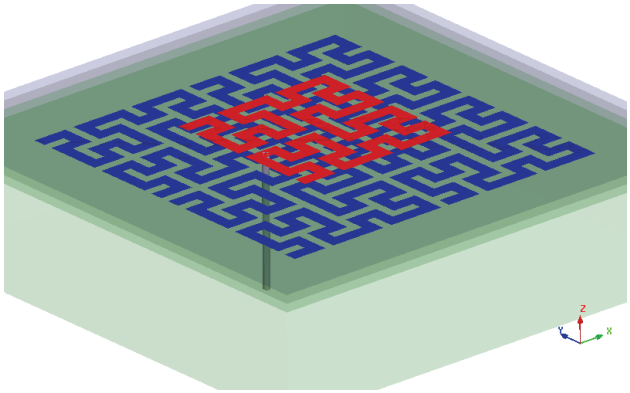

Fig. 21. Simulated model of the probe-fed Hilbert dipole antenna above a 4 element Hilbert high-impedance ground-plane.

The fabricated design is shown in Fig. 22. It should be noted that due to the Duroid substrate of the antenna, the 4-element high impedance surface is not visible in the figure. The return loss (S_{11}) results of the numerical model and the experimental prototype are shown in Fig. 23. As can be seen there is a very close agreement between the two. An additional drop is seen in the return loss of the prototype at 650 MHz, which is most likely due to some fabrication or construction flaw. This additional drop is still not in the matched range where the return loss is less than -10 dB. The resonance of interest here is the resonance which is closely correlated between both results, both in the resonant frequency and in the level of the return loss, at 700 MHz. As was previously mentioned, the antenna was designed around this 700 MHz frequency region such that the probe diameter could be inserted through the high-impedance surface level. Due to the fact that the frequency range of this design, falls outside that of our laboratory's anechoic chamber, which has a lower cut-off of 2.0 GHz, pattern measurements were not possible. The simulated gain patterns however indicated a dipolar radiation pattern, as expected, with a gain of 4.22 dBi and a bandwidth of about 0.3%. These values all correspond very closely to the values in the previous section, which assumed a perfect gap-source and identical dimensions.

Fig. 22. Prototype of the probe-fed Hilbert antenna above a 4-element Hilbert high-impedance ground-plane.

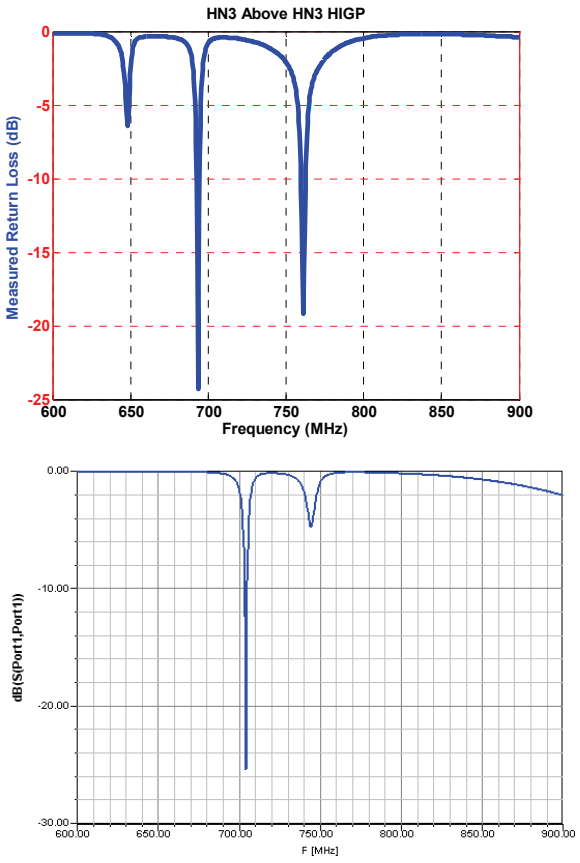

Fig. 23. Measured and simulated return loss of the fabricated Hilbert antenna above Hilbert high-impedance ground-plane.

VII. CONCLUSIONS

Arrays of Peano and Hilbert space-filling curve elements are proposed for potential use as RFID tags. Using both numerical simulations and RCS measurement, it was shown that these electrically compact resonators could produce relatively large scattered fields over an inherently narrow frequency band at their corresponding fundamental resonant modes. These tags were also investigated in terms of their performances when placed near a typical inventory objects, such as paper rolls. In addition, the use of a Hilbert-curve antenna above Hilbert AMC ground-plane was investigated for tagging of metallic objects, where it was shown that a such a configuration could provide a compact, low-profile and highly efficient technique for RFID tagging in presence of conducting surfaces.

REFERENCES

[1] J. Landt, "The History of RFID", *IEEE Potentials,* vol. 24, no. 4, pp. 8-11, Nov. 2005

[2] R. Weinstein, "RFID: A technical overview and its application to the enterprise", *IT Professional,* vol. 7, no. 3, pp. 27-33, June 2005.

[3] H. Sagan, *Space-Filling Curves,* Springer-Verlag, 1994.

[4] K. J. Vinoy, K. A. Jose, V. K. Varadan, and V. V. Varadan, "Hilbert curve fractal antenna: A small resonant antenna for VHF/UHF applications," *Microwave and Optical Technology Letters,* vol. 29, no. 4, pp. 215-219, May 2001.

[5] S. R. Best, "A comparison of the performance properties of the Hilbert curve fractal and meander line monopole antennas," *Microwave and Optical Technology Letters,* vol. 35, no. 4, pp. 258-262, November 20, 2002.

[6] J. Zhu, A. Hoorfar, and N. Engheta, "Bandwidth, cross-polarization, and feed-point characteristics of matched Hilbert antennas," *IEEE Antennas and Wireless Propagation Letters,* vol. 2, pp. 2-5, 2003.

[7] D. H. Werner and S. Ganguly, "An Overview of Fractal Antenna Engineering Research," *IEEE Antennas & Propagation Magazine,* vol. 45, no. 1, pp. 38-56, February 2003.

[8] J. Zhu, A. Hoorfar, and N. Engheta, "Peano antennas," IEEE Antennas and Wireless Propagation Letters, vol. 3, pp. 71-74, 2004.

[9] R. Olmi, M. Tedesco, C. Riminesi, and A. Ignesti, "Thickness independent measurement of the permittivity of thin samples in the X band," Measurement Science and Technology, vol. 13, pp. 503-509, 2002.

[10] J. A. McVay, K. M. Yemelyanov, A. Hoorfar, and N. Engheta, "Through-the-Wall Imaging and Sensing: An Electromagnetic Perspective," *IEEE Workshop on Signal Processing Applications for Public Security and Forensic (SAFE-2007),* April 2007.

[11] J. McVay, N. Engheta, and A. Hoorfar, "High Impedance Metamaterial Surfaces Using Hilbert-Curve Inclusions," *IEEE Microwave and Wireless Components Letters,* vol. 14, no. 3, March 2004.

[12] J. McVay, A. Hoorfar, and N. Engheta, "Peano High Impedance Surfaces," *Radio Science,* vol. 40, pp. 1-9, September 2005.